nature materials

LETTERS

PUBLISHED ONLINE: 6 APRIL 2009; CORRECTED ONLINE: 14 APRIL 2009 | DOI: 10.1038/NMAT2420

Ultralong spin coherence time in isotopically engineered diamond

Gopalakrishnan Balasubramanian[1], Philipp Neumann[1], Daniel Twitchen[2], Matthew Markham[2], Roman Kolesov[1], Norikazu Mizuochi[1,3], Junichi Isoya[3], Jocelyn Achard[4], Johannes Beck[1], Julia Tissler[1], Vincent Jacques[1], Philip R. Hemmer[5], Fedor Jelezko[1]* and Jörg Wrachtrup[1]*

As quantum mechanics ventures into the world of applications and engineering, materials science faces the necessity to design matter to quantum grade purity. For such materials, quantum effects define their physical behaviour and open completely new (quantum) perspectives for applications. Carbon-based materials are particularly good examples, highlighted by the fascinating quantum properties of, for example, nanotubes[1] or graphene[2]. Here, we demonstrate the synthesis and application of ultrapure isotopically controlled single-crystal chemical vapour deposition (CVD) diamond with a remarkably low concentration of paramagnetic impurities. The content of nuclear spins associated with the ^{13}C isotope was depleted to 0.3% and the concentration of other paramagnetic defects was measured to be $<10^{13}\,cm^{-3}$. Being placed in such a spin-free lattice, single electron spins show the longest room-temperature spin dephasing times ever observed in solid-state systems ($T_2 = 1.8$ ms). This benchmark will potentially allow observation of coherent coupling between spins separated by a few tens of nanometres, making it a versatile material for room-temperature quantum information processing devices. We also show that single electron spins in the same isotopically engineered CVD diamond can be used to detect external magnetic fields with a sensitivity reaching $4\,nT\,Hz^{-1/2}$ and subnanometre spatial resolution.

Solid-state technologies exploring quantum physics require dedicated types of material. Whereas classical semiconductor materials have had more than five decades of development with respect to purity and structure, carbon-based materials are a relatively new class of substances to this field. As spins are prominent solid-state quantum bit candidates, research on carbon systems, such as fullerenes[3,4], nanotubes[5], graphene[2] or recently diamond[6], is often driven by the requirements of having a spin-free lattice. The most abundant isotope of carbon, ^{12}C (98.9%), is nuclear spin free. Thus, carbon materials are among a limited family of substances (including Si and Ge) that can be engineered to contain a very low level of nuclear spins, in contrast to GaAs, for example. Starting with a spin-free lattice provides an excellent opportunity for subsequent spin-state quantum engineering. Diamond's recently reported long phase memory and relaxation times as a result of the low natural spin abundance[6] makes it ideally suited for high-sensitivity applications such as metrology and microscopy[7,8]. The availability of an optical read-out for single spins associated with colour centres is another crucial building block for quantum information processing applications[9–11].

The present experiments use spins associated with nitrogen-vacancy defects to probe the paramagnetic properties of the host material. The nitrogen-vacancy defect is a well-studied impurity in diamond that comprises a substitutional nitrogen and a next neighbour vacancy (see Fig. 1a) with an electron paramagnetic $S = 1$ electron spin ground state. The fluorescence intensity depends on the spin state of the defect and hence the electron spin resonance signal of single defects can be read out.

The single-crystal diamond samples studied here were synthesized with a microwave plasma-assisted chemical vapour deposition (CVD) reactor operating at a frequency of 2.45 GHz. Homoepitaxial CVD diamond layers were deposited onto specially prepared ⟨100⟩-oriented diamond substrates[12]. Care was taken to ensure that the surface quality of the substrates was as high as possible to minimize the dislocations in the epitaxial layer. The challenge in achieving isotopic enriched diamond is to reduce the incorporation of other paramagnetic impurities while using isotopically purified starting material. Isotopic enrichment was accomplished by using purifiers to reduce non-intentional dopants and isotopically enriched methane at 99.7% in a hydrogen environment (95% by composition). These conditions led to samples in which the paramagnetic impurity concentration (including nitrogen, hydrogen and silicon defects) was minimized. Intrinsic nitrogen can recombine with vacancies during the growth process with a yield of a few per cent, leading to formation of nitrogen-vacancy centres at a concentration suitable for single centre selection using standard confocal microscopy. Figure 1b shows confocal microscopy images of CVD diamond with well-resolved single nitrogen-vacancy defects. By counting single defects in a confocal plane, we estimate the concentration of nitrogen-vacancy defects to be of the order of $10^{10}\,cm^{-3}$. By using a rough estimate for the nitrogen to nitrogen-vacancy conversion ratio of one per cent[13], confocal microscopy gives an approximate value for the nitrogen impurity concentration of 5×10^{-2} ppb (below the detection threshold using conventional ensemble spin resonance methods or other bulk techniques such as secondary-ion mass spectrometry).

At such a low concentration of paramagnetic impurities, ultrapure CVD diamond has the potential to become a new class of material in which spin quantum effects could be observed at room temperature over hundreds of nanometres. Placed in a

[1]3 Physikalisches Institut, Universität Stuttgart, 70550 Stuttgart, Germany, [2]Element Six Ltd, King's Ride Park, Ascot SL5 8BP, UK, [3]Graduate School of Library, Information and Media Studies, University of Tsukuba, 1-2 Kasuga, Tsukuba, Ibaraki 305-8550, Japan, [4]LIMHP/CNRS, Université Paris 13, 93430 Villetaneuse, France, [5]Texas A&M University, College Station, Texas 77843, USA. *e-mail: f.jelezko@physik.uni-stuttgart.de; wrachtrup@physik.uni-stuttgart.de.

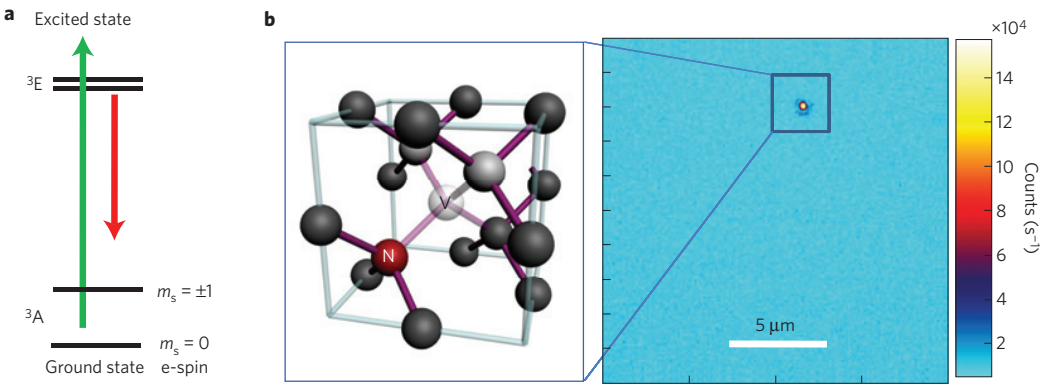

Figure 1 | Nitrogen-vacancy defect in diamond. a, Structure and energy level scheme of the nitrogen-vacancy defect in diamond. **b**, Fluorescence microscopy image of high-purity CVD diamond containing single nitrogen-vacancy defects. Fluorescence is encoded in the colour scale.

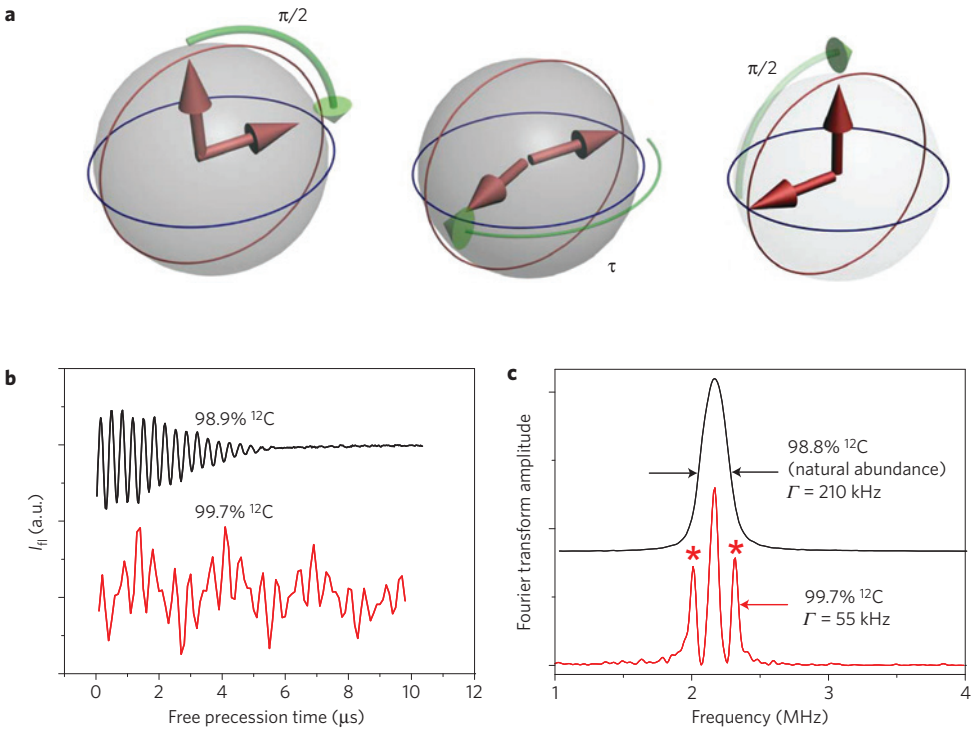

Figure 2 | Coherence time of single spins. a, Schematic diagrams of the FID experiment. The electron spin state is represented as a vector on a Bloch sphere with eigenstates pointing in the direction of the poles. **b**, FID signal measured on a single nitrogen-vacancy electron spin for diamond with a natural abundance of ^{13}C isotope (black curve, ^{12}C content 0.989) and isotopically engineered crystal (red curve, ^{12}C concentration 0.997). The applied magnetic field was 690 G. **c**, Fourier-transform spectra of FID signals. The satellites indicated by asterisks are related to the hyperfine interaction with the nitrogen and carbon nuclei. Note that two out of three hyperfine components associated with ^{14}N nuclei of nitrogen-vacancy defects are present in the spectral range shown in the figure. Extra splitting resulting in a triplet is associated with distant ^{13}C nucleus splitting.

coherent superposition of spin-up and spin-down states, a single impurity spin will usually lose its phase quickly, owing to interaction with other spins and phonons present in the lattice. Owing to strong binding between low-mass carbon atoms, diamond has some outstanding properties in this respect, with phonon-limited spin-lattice relaxation times around 10^2–10^4 s. This means that the phase coherence time of electron spins in room-temperature diamond is not limited by spin-lattice interactions (as is the case in other materials), but rather governed by dipolar interactions with other spins. Dipolar coupling to electron spins can be neglected because of the large distances to neighbouring nitrogen impurities (a few micrometres for the estimated 10^{-2} ppb concentration in our material). Hence, the main source of electron spin decoherence is the nuclear spin bath arising from the presence of ^{13}C atoms. To exemplify this effect, we show the electron spin resonance linewidth of a single nitrogen-vacancy defect centre as a function of ^{13}C concentration (Fig. 2). Spectra recorded by acquiring the free induction decay (FID) signal of the single electron spin show that as the ^{13}C nuclear spin concentration is diminished, the electron spin linewidth is drastically reduced. Indicative of the small linewidth is the comparatively long decay time of the FID of tens of microseconds. The full-width at half-maximum linewidth in the spectrum shown in Fig. 2 is 55 kHz, which is the smallest single electron spin resonance linewidth ever measured in a solid-state material. The full-width at half-maximum of the electron spin resonance line of a single defect is related to the ^{13}C concentration by $\delta = (2/\pi)\sqrt{2M_2}$, with M_2, the second moment of the electron spin resonance line, being $M_2 \propto (1/5) f \gamma_C^2 \hbar^2 \sum_k r_k^{-6}$, where the summation is over all ^{13}C nuclei, f is the abundance of ^{13}C nuclei, γ is the nuclear spin gyromagnetic ratio and r_k is the distance between electron and ^{13}C nuclear spins. From this we can estimate the abundance of ^{13}C as measured by electron spin resonance to be 0.5%, which is in

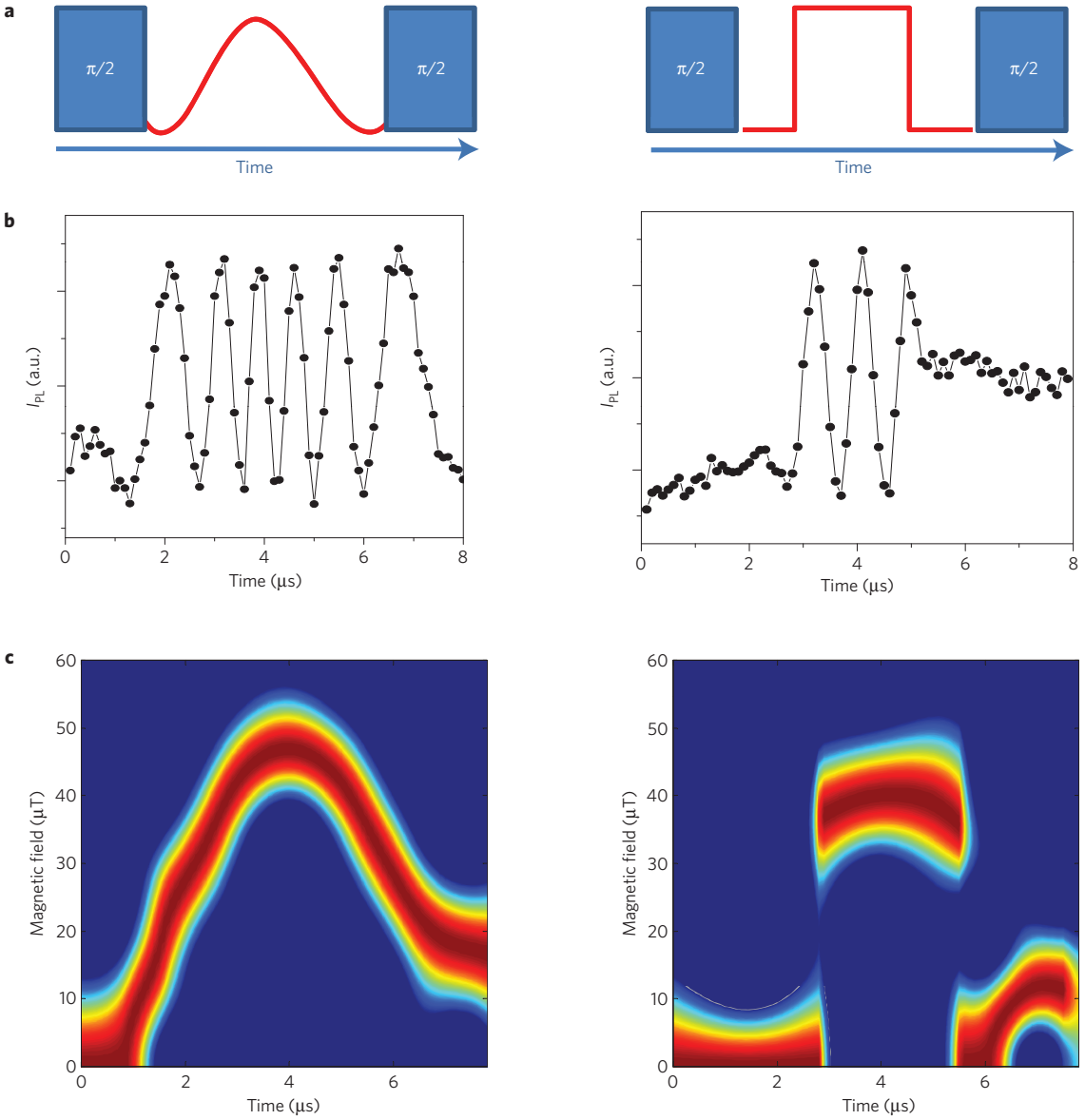

Figure 3 | Diamond magnetometry. a, Diagrams of magnetic field measurements using single spins associated with defects in diamond. **b**, Experimental data showing accumulation of the phase of the FID resulting from an applied magnetic field. **c**, Reconstructed magnetic field profiles. The two test patterns presented are a sine wave (left) and a square pulse (right).

qualitative agreement with the concentration of ^{13}C impurities in the enriched methane used for the diamond growth (0.3%).

The low 'intrinsic spin noise' of the ultrapure diamond material renders the nitrogen-vacancy defect to be a sensitive detector for external magnetic fields. Owing to its atomic size, such a nitrogen-vacancy magnetic field sensor would provide unprecedented performance, both in sensitivity (that is, $\Delta B\sqrt{t}$, where ΔB is detectable change of magnetic field within time t) and in spatial resolution. External magnetic fields shift electron spin resonance lines according to $h\nu = g\mu_B B_0$, where B_0 is the external magnetic field. With a linewidth of about 50 kHz, an external field of 20 mG would be detectable as a line shift. The most straightforward way to measure such a line shift is to use Ramsey fringes as a detection method. In this approach, two $\pi/2$ microwave pulses are separated by a free precession period τ. The accumulated phase difference is

$$\Delta\phi = \frac{g\mu_B}{\hbar}\int_0^{\tau} B(\tau)\,\mathrm{d}t \qquad (1)$$

Figure 3 shows an example of such a field measurement. Initially τ is chosen such that the fluorescence corresponds to a maximum amplitude of the Ramsey fringes. Switching on $B(t)$ during the free precession interval causes oscillations of the read-out signal, indicating an accumulation $\Delta\phi$. A wavelet transform recovers the time variation of the magnetic field (see Fig. 2). Two factors affect the accuracy of the field measurements. First, the field sensitivity is proportional to the slope of the Ramsey fringes, which is given by $g\mu_B\tau/\hbar$. Second, as the magnetic resonance signal is detected optically, photon shot noise affects accuracy. The standard deviation of photon number Δn depends on the average number of photons $\langle n\rangle$ as $\Delta n = \sqrt{\langle n\rangle}$. Hence, on increasing the free precession time interval, less photons are collected for a given measurement time, but the noise scales as $\sqrt{\tau}$. When combining both error sources, we conclude that sensitivity depends on the free precession time as $1/\sqrt{\tau}$. As a result, the ultimate sensitivity is given by the maximum value of τ, which is limited by the coherence time T_2^*. This phase memory time T_2^* determines the full (inhomogeneous) linewidth of the spin resonance transition, which is usually much larger than the homogeneous linewidth (T_2). Below, we show

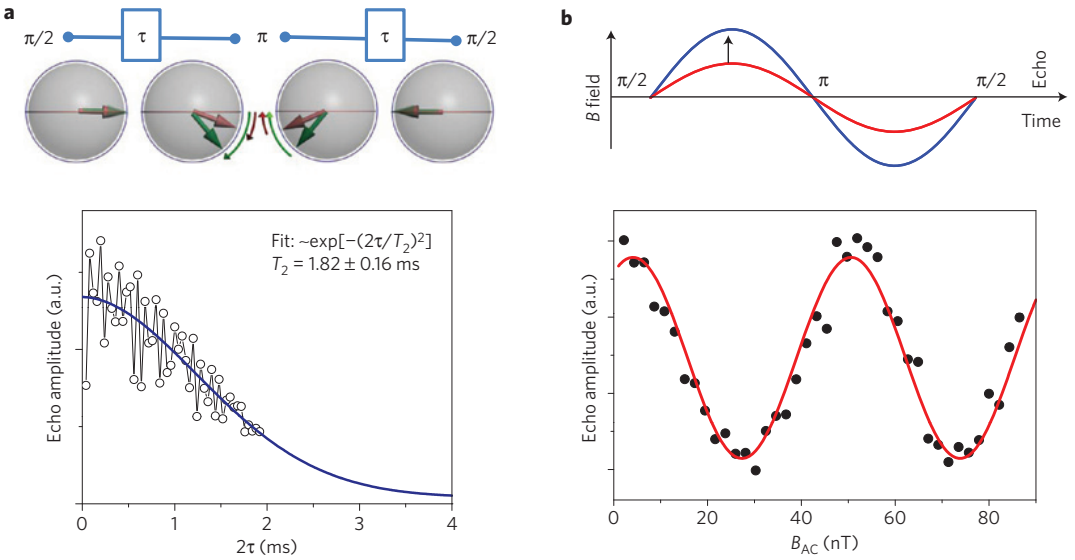

Figure 4 | Measurement of an external magnetic field using the spin echo technique. a, Spin coherence time of single spins in isotopically engineered diamond measured using a two-pulse electron spin echo. The upper panel shows the evolution of the Bloch vector during the echo pulse sequence. The lower graph shows the decay of spin echo as a function of inter-pulse distance. **b**, The upper panel shows the pulse diagram and the temporal evolution of the external magnetic field for the a.c. magnetometry experiments. The lower graph shows experimental data on the phase accumulation of the electron spin induction phase on increasing the external magnetic field strength. The error for the fit function corresponds to a sensitivity of 4 nT $Hz^{-1/2}$.

that coherent control of the electron spin can greatly improve the magnetic field measurement effectively by extending the observation time from T_2^* to T_2. Owing to the long correlation times for the dipolar interactions between nuclear spins in diamond, a spin echo can markedly enhance the observed coherence time by coherently averaging out local or global magnetic field fluctuations on a timescale longer than the dwell time of the echo (2τ). Using this technique, the pure dephasing time of the nitrogen-vacancy centre electron spin echo, T_2, is revealed. Defects in the isotopically purified sample show dephasing times between 0.5 ms and 2 ms. The echo decay of a particular single electron spin in our ultrapure CVD diamond sample is shown in Fig. 3. The echo decays on a timescale of 1.8 ms, the longest echo decay time measured for this system so far. Converting the echo decay time into a homogeneous linewidth recovered by the two pulse echo gives $\Delta\nu = (1/\pi T_2) = 180$ Hz.

Clearly, in the absence of electron spin impurities, carbon nuclear spins dominate the dephasing behaviour of the electron spin, similar to their contribution to T_2^*, the inhomogeneous linewidth discussed above. Even in a dilute lattice of ^{13}C nuclei, there is a residual mutual magnetic dipole coupling among individual ^{13}C nuclei in the lattice. For a dilute spin system, the typical distance between neighbouring nuclei can be derived from a Poissonian distribution, $e^{-4\pi N_C r_{jk}^3/3}$, of finding no other particle, k, within a distance, r_{jk}, of particle, j, equal to 1/2. This gives $r_{jk} = 0.55 N_C^{-1/3}$, where N_C is the concentration of ^{13}C nuclei (in atoms cm^{-3} units). Assuming an external magnetic field parallel to the z axis of the nitrogen-vacancy defect, the I_{xy} part of the nuclei interaction Hamiltonian (which causes dynamics of the ^{13}C nuclear spin bath) then leads to flip-flop processes, where two nuclei exchange their I_z components. This causes a fluctuating magnetic field that is responsible for dephasing of the electron spin. Using this information, the mean interaction strength can be calculated to be 500 Hz for 0.3% of ^{13}C, which is in good agreement with the echo decay data presented in Fig. 4. A more detailed numerical analysis of electron spin decoherence interacting with a ^{13}C spin bath is given by, for example, Maze *et al.*[14].

The maximum B field sensitivity is achieved in an a.c. magnetic field, changing its sign at time τ when the refocusing pulse of the echo is applied. As a result of this pulse sequence, the electron spin acquires an extra phase at the time of echo detection according to equation (1), with the sensitivity given by $\Delta B = \pi\hbar/g\mu_B\sqrt{T_2}$. The improvement in sensitivity arises from increasing the interrogation time from T_2^* to T_2 (see Fig. 4b). Changing the magnetic field results in a periodic modulation of the magnetometer signal[8] owing to the fact that the increased phase, $\Delta\phi$, is projected to the measurement axis on read out of the magnetometer. The maximum sensitivity of this measurement is found to be 4.3 nT $Hz^{-1/2}$, which is close to one order of magnitude improvement compared with previously reported measurements using ultrapure diamond with natural ^{13}C abundance[8].

The ability of ultrapure isotopically controlled CVD diamond to detect weak magnetic fields with high local resolution might have implications in, for example, life science. An example of which are diamond magnetometers used to detect magnetic fields associated with the ion flow through membrane channels in cells. Another example, owing to their coherent dipolar coupling, is to create an array of nitrogen-vacancy centres that would present an intriguing room-temperature quantum device for quantum computing applications, simulation of phase transitions and so on. For such a device, the maximum spacing between nitrogen-vacancy centres can be estimated by considering the case when the magnetic field created by a single nitrogen-vacancy spin, which is given by $B_{dip} = \sqrt{2}(\mu_0\mu/4\pi)(\sqrt{3\cos^2\vartheta + 1}/r^3)$ (here μ is the magnetic moment of a single electron spin), causes a shift of the electron spin resonance lines that exceeds its linewidth. Substitution of the relevant values ($\mu = 10^{-23}$ J T^{-1}) gives a field of 10^{-9} T produced by a single nitrogen-vacancy spin at a distance of roughly 100 nm. Using this value, we conclude that with the current limit in dephasing times, two nitrogen-vacancy electron spins, at a distance of 100 nm, will be coherently coupled. This distance is sufficient for the two centres to be addressed and read out separately by modern methods of nonlinear optical microscopy and also manufacturable with current implantation techniques that allow some 10 nm precision[15].

As the distance at which coherent coupling prevails scales as $\sqrt[3]{N_C}$, a further reduction of the ^{13}C concentration by one order of magnitude would enable an increase of the mutual separation by roughly a factor of 2. The maximum distance is limited by the electron spin relaxation time, the value of which was assumed

to be 1.8 ms. Note that the ultimate limit for the coherence time of a spin-free diamond host is given by spin-lattice relaxation, which is expected to occur in a seconds timescale. In this case, micrometre-scale-separated electron spins would show coherent coupling, an almost macroscopic scale quantum array.

Methods

Magnetic resonance on single spins. Magnetic resonance measurements on single nitrogen-vacancy defects were carried out using a home-built confocal microscope. Single nitrogen-vacancy defects were excited by a continuous-wave solid-state 532 nm laser source. Laser light was focused on single defects using a high-numerical-aperture microscope objective lens. Fluorescence was collected through the same objective and filtered from excitation light using a long-pass interference filter. Excitation of the electron spin resonance transitions of single defects was carried out by passing microwaves through a thin wire located close to the sample. Magnetometry measurements were carried out by applying magnetic fields and recording the FID or Hahn echo. The temporal evolution of spin dephasing resulting in florescence signal oscillation carries the information on the time-varying magnetic field within the free precession interval. The encoded signal is deconvolved using time-frequency distribution to retrieve the magnetic field variation at every instant of time. The discrete time–frequency analysis is done using Matlab toolboxes and custom-written codes. The sensitivity for a.c. magnetic field measurements was derived from the standard deviation of the fit function of experimental data points (Fig. 4b).

Calculation of spin-lattice relaxation times. Spin relaxation related to the lattice is weak in diamond even at room temperature, because only lattice vibrations with frequency matching the Larmor frequency of the electron spins can induce a spin flip. The rate for this direct process is $(1/T_1) = (54\pi v^2/\hbar\rho v_0^5)(\mu_B^2/r_0^3)^2 kT$ (ref. 16), where ρ is the mass density, v is the oscillator frequency, v_0 is the velocity of sound, r_0 is the lattice separation of neighbours and μ_B is the Bohr magneton[17]. Substituting the relevant values for diamond, yields $T_1 = 10^4$ s for $T = 300$ K. Alternatively, an electron spin flip could be induced by inelastic scattering of a higher frequency lattice phonon (Raman process). The relaxation rate in this case is given by $(1/T_1) = (163\pi^2 6!/\rho^2 v_0^{10})(\mu_B^2/r_0^3)^2 (kT/h)^7$ (for details, see ref. 16). Substitution of the relevant values yields $T_1 = 10^2$ s. Other mechanisms such as the Orbach process require the existence of optical phonons, which under ambient conditions are not excited in diamond.

Received 21 November 2008; accepted 23 February 2009; published online 6 April 2009

References

1. Cleuziou, J. P., Wernsdorfer, W., Bouchiat, V., Ondarcuhu, T. & Monthioux, M. Carbon nanotube superconducting quantum interference device. *Nature Nanotech.* **1**, 53–59 (2006).
2. Geim, A. K. & Novoselov, K. S. The rise of graphene. *Nature Mater.* **6**, 183–191 (2007).
3. Harneit, W., Meyer, C., Weidinger, A., Suter, D. & Twamley, J. Architectures for a spin quantum computer based on endohedral fullerenes. *Phys. Status Solidi B* **233**, 453–461 (2002).
4. Benjamin, S. C. *et al.* Towards a fullerene-based quantum computer. *J. Phys. Condens. Matter* **18**, S867–S883 (2006).
5. Jorgensen, H. I. *et al.* Singlet–triplet physics and shell filling in carbon nanotube double quantum dots. *Nature Phys.* **4**, 536–539 (2008).
6. Gaebel, T. *et al.* Room-temperature coherent coupling of single spins in diamond. *Nature Phys.* **2**, 408–413 (2006).
7. Balasubramanian, G. *et al.* Nanoscale imaging magnetometry with diamond spins under ambient conditions. *Nature* **455**, 648–U46 (2008).
8. Maze, J. R. *et al.* Nanoscale magnetic sensing with an individual electronic spin in diamond. *Nature* **455**, 644–U41 (2008).
9. Childress, L. *et al.* Coherent dynamics of coupled electron and nuclear spin qubits in diamond. *Science* **314**, 281–285 (2006).
10. Dutt, M. V. G. *et al.* Quantum register based on individual electronic and nuclear spin qubits in diamond. *Science* **316**, 1312–1316 (2007).
11. Neumann, P. *et al.* Multipartite entanglement among single spins in diamond. *Science* **320**, 1326–1329 (2008).
12. Isberg, J. *et al.* High carrier mobility in single-crystal plasma-deposited diamond. *Science* **297**, 1670–1672 (2002).
13. Tallaire, A. *et al.* Characterisation of high-quality thick single-crystal diamond grown by CVD with a low nitrogen addition. *Diamond Relat. Mater.* **15**, 1700–1707 (2006).
14. Maze, J. R., Taylor, J. M. & Lukin, M. D. Electron spin decoherence of single nitrogen-vacancy defects in diamond. *Phys. Rev. B* **78**, 094303.
15. Schmidt, R. *et al.* Spherical nanosized focal spot unravels the interior of cells. *Nature Meth.* **5**, 539–544 (2008).
16. Pake, G. E. *Paramagnetic Resonance, An Introductory Monograph* (Benjamin, 1962).
17. Scott, P. L. & Jeffries, C. D. Spin-lattice relaxation in some rare-earth salts at helium temperatures—observation of phonon bottleneck. *Phys. Rev.* **127**, 32–51 (1962).

Acknowledgements

This work was supported by the EU (QAP, EQUIND, NANO4DRUGS, NEDQIT), DFG (SFB/TR21 and FOR730), Landesstiftung BW and the Volkswagen Stiftung. P.R.H. acknowledges support by the NIH and DARPA.

Author contributions

G.B., P.N., R.K., N.M., J.B., J.T., V.J., P.R.H. and F.J. carried out the experiments; D.T., M.M. and J.A. designed and carried out synthesis of diamond material. All authors discussed the results, analysed the data and commented on the manuscript. J.W. wrote the paper.

Additional information

Reprints and permissions information is available online at http://npg.nature.com/reprintsandpermissions. Correspondence and requests for materials should be addressed to F.J. or J.W.

ERRATUM

Ultralong spin coherence time in isotopically engineered diamond

Gopalakrishnan Balasubramanian, Philipp Neumann, Daniel Twitchen, Matthew Markham, Roman Kolesov, Norikazu Mizuochi, Junichi Isoya, Jocelyn Achard, Johannes Beck, Julia Tissler, Vincent Jacques, Philip R. Hemmer, Fedor Jelezko and Jörg Wrachtrup

Nature Materials **8,** 383–387 (2009); published online: 06 April 2009; corrected online: 14 April 2009.

In the version of this Letter originally published online, the family name of one of the co-authors, Norikazu Mizuochi, was spelt incorrectly; it is correct here, and has now been corrected in all versions of the Letter.